AUTHOR QUERY FORM

Dear Author,

Please check your proof carefully and mark all corrections at the appropriate place in the proof (e.g., by using on-screen annotation in the PDF file) or compile them in a separate list. Note: if you opt to annotate the file with software other than Adobe Reader then please also highlight the appropriate place in the PDF file. To ensure fast publication of your paper please return your corrections within 48 hours.

For correction or revision of any artwork, please consult http://www.elsevier.com/artworkinstructions.

Any queries or remarks that have arisen during the processing of your manuscript are listed below and highlighted by flags in the proof. Click on the Q link to go to the location in the proof.

Your article is registered as a regular item and is being processed for inclusion in a regular issue of the journal. If this is NOT correct and your article belongs to a Special Issue/Collection please contact a.arulanandaraj@elsevier.com immediately prior to returning your corrections.

Location in article	Query / Remark: **click on the Q link to go** **Please insert your reply or correction at the corresponding line in the proof**
Q1	Please confirm that given names and surnames have been identified correctly and are presented in the desired order.
Q2	The number of keywords provided exceeds the maximum allowed by this journal. Please delete one keyword.

Thank you for your assistance.

Highlights

International Journal of Rock Mechanics & Mining Sciences ∎ (∎∎∎∎) ∎∎∎–∎∎∎

A permafrost test on intact gneiss rock

Q1 S. Duca [a], E. Alonso [b], C. Scavia [c]

[a] Department of Structural, Building and Geotechnical Engineering, Politecnico di Torino, Turin, Italy
[b] Department of Geotechnical Engineering and Geo-Sciences, Universitat Politècnica de Catalunya, Carrer Jordi Girona, 1-3, Building D2, 08034 Barcelona, Spain
[c] Department of Structural, Building and Geotechnical Engineering, Politecnico di Torino, Corso Duca degli Abruzzi 24, 10129 Torino, Italy

- A laboratory test on intact hard rock, which shows that ice may segregate at a well defined position creating a discontinuity in the rock matrix. The implication is that permafrost driven rockfalls do not require the presence of previously existing rock discontinuities to become active.
- A model capable of predicting the generation of the ice segregation front with good accuracy. The model uses principles that have previously been shown to be accurate and thermodynamically sound when analyzing ice-induced heave in soils.

A permafrost test on intact gneiss rock

Q1 S. Duca [a,1], E.E. Alonso [b,*], C. Scavia [c]

[a] Department of Structural, Building and Geotechnical Engineering, Politecnico di Torino, Turin, Italy
[b] Department of Geotechnical Engineering and Geo-Sciences, Universitat Politècnica de Catalunya, Carrer Jordi Girona, 1-3, Building D2, 08034 Barcelona, Spain
[c] Department of Structural, Building and Geotechnical Engineering, Politecnico di Torino, Corso Duca degli Abruzzi 24, 10129 Torino, Italy

ARTICLE INFO

ABSTRACT

Changes in permafrost conditions in high mountain rocks have increased the risk of dangerous instabilities. Ice segregation within the rock mass has been interpreted as one of the mechanisms involved in high mountain bedrock degradation. A long term laboratory test on a cube of intact gneiss has been designed to reproduce field temperature gradients and water supply conditions. Test results demonstrate that ice crystallization in a permafrost fringe ($T=0\ ^{\circ}C$ to $-3\ ^{\circ}C$) leads to the formation of continuous ice-filled cracks which explain the loss of rock continuity and the observed rock failures. A coupled thermo-hydro-mechanical model which incorporates the thermodynamics of ice-water mixtures has been used to reproduce test results. The model, which follows existing formulations for unsaturated porous media, was capable of capturing the main observations derived from the experiment. Calculated tensile stresses are close to the gneiss tensile strength. The analysis performed is a step forward in understanding field observations and in the application of computational tools to real cases.

© 2015 Elsevier Ltd. All rights reserved.

1. Introduction

Degrading permafrost in rock walls is considered to be an increasing hazard in alpine environments. It results in rockfall activity and slow rock deformation which endangers infrastructure and people [1]. The increasing importance of hydro-electric power generation and storage in high topography settings and the high-alpine winter and adventure tourism increases the vulnerability to permafrost rock slope failure and requires improved assessment and monitoring strategies for permafrost rock walls [2].

It has been postulated that permafrost distribution responds quickly to climatic fluctuations [3] Detachment zones of rock-ice avalanches indicate thermal disturbances caused by the interaction of permafrost, glacial ice, and climate changes. Krautblatter [1] explained how permafrost dynamics influence rock slope stability by reducing shear resistance. Fischer et al. [4] modeled the effects of enhanced hydrostatic pressure due to a perched water level sealed by permafrost. Upward freezing due to ice segregation could cause the propagation of ice-filled fractures, which may provide a slip plane during thawing [5]. While macrogelivation (frost wedging) is postulated to operate in rock

discontinuities close to the surface [6], microgelivation (i.e. ice in pores and ice segregation) could physically operate at depths of several meters, where permafrost is found in Alpine environments. In this context, the processes and mechanical understanding of the permafrost-related failure mechanisms is also a crucial issue to decipher its impact among multiple other factors that influence rock slope stability.

Many ice-rock avalanches have been documented in the Italian Alps [7], e.g. Brenva, 1997; Grandes Jorasses, 2002; Matterhorn, 2003; Thurwieserspitze, 2004; Dru, 2005; Aiguille des Toules, 2008; Tré-la-Tête, 2008; Patrí Peak, 2008; Refuge Vittorio Emanuele II, 2008; Mont Crammont, 2008; Aiguille du Dru, 2011. Enhanced activity of cliff falls, block falls, boulder falls and debris falls has been observed from permafrost-affected rock faces [8–11].

The awareness of rock slope instabilities in high mountain environments raised in alpine European countries after summer 2003 when an exceptional heat wave hit central Europe and was accompanied by an unusually high number of rock-falls [12].

Focusing on the Italian Alpine region, the Matterhorn (4478 m a.s.l., NW Italian Alps), a rock pyramid made of highly fractured gneisses and gabbros, has suffered rock deformation and rock-falls since summer 2003.

The most relevant rockfall event in the area, the "Cheminée" rockfall (2000 m³), occurred on August 18th 2003, just below the Carrel hut [13]. The presence of massive ice in the detachment zone (15 m high and 7 m large), has been interpreted as a signal of

an ice segregation mechanism involved in high mountain bedrock degradation.

The original idea of this study was indeed that rock mass instabilities could be related to the failure of intact rock bridges connecting non-persistent discontinuities, often conditioned by subcritical crack growth. From a mechanical point of view, the presence of permafrost could increase tensile normal stress due to changing water pressure and cryostatic pressure, provided by ice segregation phenomena. Then, a "layer" of segregated ice may reduce substantially the original rock shear strength and explain the failure. The segregation of ice in undamaged rock exposed to permafrost and a source of external water (rainfall in the field) will be examined in this paper through a laboratory experiment mimicking field conditions. The experiment will be interpreted with a coupled THM model for simultaneous water transfer and ice formation in porous rock

2. Ice segregation and rock fracture

A monitoring system composed by geophones and thermometers was installed at the Carrel hut within the framework of a European Community funded project (Interreg IIIA Alcotra project "PERMAdataROC"), which enabled the performance of crossed analysis between microseismic data and thermal analysis. A simplified heat-transfer numerical model was developed by Duca [14] in order to assess if the superficial source location obtained from microseismic monitoring could be correlated to the bedrock thermal regime.

Comparing the two spatial–temporal distributions of temperature and microseismic activities, it has been possible to verify that the microseismic recorded data could be correlated with thaw and solidification mechanisms. The thermal profile obtained from the numerical model showed that the rockwall located at 3829 m a.s.l. experiences a seasonal frost/thaw penetration, 2 m deep, and the microseismic source location has revealed that sources were concentrated in the active layer. In particular, the hypocenters of a selected class of nine events, which may belong to a discontinuity system, seemed to be localized close to the permafrost boundary, a layer characterized by ice-rich fractured zones and ice-filled cracks.

These results could confirm the hypothesis of ice segregation as a mechanism leading to steep bedrock degradation and its associated instability. This process could contribute to the destabilization of much larger volumes of rock than would be expected due to ice volumetric expansion.

Ice segregation is an alternative process of bedrock fracture: it occurs when temperature gradient-induced suction in freezing or frozen ground (or rock) drives unfrozen water (held in capillaries and adsorbed on the surfaces of mineral particles) through a porous medium towards a freezing site, where lenses or layers of ice grow. At subfreezing temperatures, domains that are cold enough to allow sufficient ice-generated pressure, cause progressive microcrack growth. If ice segregation fractures bedrock permafrost, the fractures and ice lenses are expected to concentrate just beneath the top of the permafrost and at the bottom of the active layer [15]. The unfrozen water, held in capillaries and adsorbed on the surfaces of mineral particles, is driven by temperature gradient-induced suction toward freezing sites where lenses or layers of ice grow. The resulting heaving pressure is nearly twice as large as the tensile strength of the stronger rocks.

This phenomenon provides the initial incentive for developing the segregation ice model of frost weathering [16], as it implies that ice growth in pre-existing microfractures is capable of progressively fracturing any rock type.

Field monitoring has highlighted the roles of diurnal and annual frost cycles in controlling the timing and magnitude of frost weathering. In the laboratory, bidirectional freezing in soft, porous rocks has produced fractures containing segregated ice layers near the permafrost table, which imply the development of ice-filled fractures in permafrost bedrock over long time-scales. This finding, combined with numerical modeling of the thermal regime in permafrost rock slopes, contributes to the prediction of large-scale rockfalls and rock avalanches triggered by permafrost degradation [5]. These authors also suggested that future studies should also focus on explosive shattering, frost weathering of hard-intact rocks, field monitoring of ice segregation and bedrock heave, and the role of frost weathering in landscape evolution.

Concerning frost weathering of hard rocks in high mountains, they proposed a question to be answered: "Does microgelivation of hard intact rocks require an extant microcrack system developed by any process or inherited?" [17].

Laboratory freeze-thaw tests have never proved the generation and propagation of new, visible cracks in hard intact rocks; they have only revealed a minor decrease in ultrasonic velocity or Young's modulus, or a minor increase in porosity [17–19]. The ice-segregation theory suggests that cracks in such low-porosity rocks (e.g. granite) propagate at low temperatures i.e. $-4\,°C$ to $-15\,°C$ [16], but laboratory simulations have so far induced ice segregation at higher temperatures ($> -2\,°C$) in high-porosity rocks (tuff and chalk).

In order to deepen the study of ice segregation phenomenon and resulting crack growth in hard, intact rock, a down scaled physical simulation of this frost weathering mechanism has been designed and set up: upsizing of physical modeling experiments and monitoring natural unweathered bedrock, would provide valuable insights into permafrost landscape evolution and engineering geology.

This paper presents also a numerical analysis of the test performed in an effort to improve process understanding and to develop predictive tools. These studies have addressed the mechanics of ice growth, particularly the role of the pre-melted films in lens growth, and the fracturing mechanism in rock under steady temperature gradients.

3. Thermo-hydro-mechanical (THM) analysis of frozen rock

Freezing of pore fluid within rock microcracks involves complex thermal, hydraulic and mechanical processes that can have significant mutual interactions. For example, phase changes of pore fluid caused by temperature variations modify the hydraulic regime of the material, which in turn induces mechanical deformation. At the same time, any change in the hydraulic and mechanical conditions feeds back to the thermal processes by way of advection and changes in ice and water contents [20].

Analysis of frozen rock behavior inevitably requires a numerical technique because of the non-linearity of the governing equations. Models have been developed and implemented with differing hypotheses and degrees of sophistication [14].

In order to predict the approximate depth of maximum cracking for an upward freezing experiment described below, a fully coupled thermo-hydro-mechanical (THM) model, whose basic formulation was described in [21,22], has been applied. The concept accepted is that freezing in water saturated rocks is closely analogous to slow freezing in fine grained soils. In fact assuming an initially uniform distribution of very small defects throughout the block, the gneiss sample has been considered as an "equivalent porous medium" characterized by its porosity, and a set of thermo-mechanical properties.

Ice segregation processes are caused by water migration and accumulation in a frozen fringe (i.e. a transitional zone just behind a freezing front, where rock is partially frozen). The water migration is driven by cryogenic suction but at the same time it is retarded by the reduced permeability developed in the partially frozen rock.

3.1. Governing equations

The frozen soil formulation presented builds from the THM modelling by [21–23], originally developed for high-temperature problems involving a gas phase (unsaturated soils). Low-temperature problems can be considered to be modeled by the same overall structure if the original gas phase is replaced by a new solid phase representing ice [20]. The formulation has been implemented in the FEM code CODE_BRIGHT, a program for thermo-hydro-mechanical analysis in geological media, considering the new features required to address freeze/thaw conditions.

3.2. Thermodynamic equilibrium of freezing soil

The equilibrium between liquid water (l) and ice (i) phases is described by the Clausius–Clapeyron equation, derived from equilibrium of the chemical potentials between two phases:

$$-(s_l - s_i)dT + \nu_l dP_l - \nu_i dP_i = 0 \tag{1}$$

where s and ν are the specific entropy and the specific volume respectively, T is temperature on the thermodynamic scale, and P is pressure.

From Eq. (1),

$$dP_i = \frac{\rho_i}{\rho_l}dP_l - \frac{\rho_i L}{T}dT \tag{2}$$

where L is the specific latent heat of fusion and ρ $(1/\nu)$ is the mass density. This differential form can be integrated taking atmospheric pressure and the temperature 273.15 °K as references, to give:

$$dP_i = \frac{\rho_i}{\rho_l}dP_l - \rho_i L \ln\left(\frac{T}{273.15}\right) \tag{3}$$

This equation represents a thermodynamic requirement for equilibrium that needs to be satisfied by P_i, P_l and T [20].

3.3. Freezing characteristic function

The model requires a freezing characteristic function to relate the degree of liquid (unfrozen water) saturation S_l (i.e. volume of liquid phase/volume of pore) to the porous medium thermodynamic properties [20]. Many researchers have developed freezing characteristic functions through analogies with water retention models developed to describe the drying and wetting of unsaturated unfrozen soils, where gas and liquid phases coexist in the pores [24–28]. The different pressures between the liquid water and ice phases expressed by the Clausius–Clapeyron Eq. (3) suggest that surface tension forces should develop along the interface between the two phases.

The freezing characteristics and the water retention characteristics are both determined by the pore size distribution [28,29] and the interface tension force. It is therefore natural to assume that the two functions can be expressed by similar forms of equations, once allowance is made for the difference between the ice/liquid and gas/liquid interface tension forces. The van Genuchten model [30] was used here to represent the freezing characteristic function:

$$S_l = \left[1 + \left(\frac{P_i - P_l}{P}\right)^{\frac{1}{1-\lambda}}\right]^{-\lambda} \tag{4}$$

where P and λ are material constants. This equation represents the relationship between P_i, P_l and S_l.

By combining Eqs. (3) and (4), the freezing characteristic function relating S_l to T can be obtained as:

$$S_l = \left\{1 + \left[\frac{-(1-\rho_i/\rho_l)P_l - \rho_i l \ln(T/273.15)}{P}\right]^{\frac{1}{1-\lambda}}\right\}^{-\lambda} \tag{5}$$

During prolonged freezing, water migrates and could be accumulated in a frozen fringe, i.e. a transitional zone just behind a freezing front, where the porous material is partially frozen (see Fig. 1). The water migration is driven by the cryogenic suction $(P_i - P_l)$.

Balance laws for mass and heat transfer are required dealing with a boundary value problem, together with the definition of some additional constitutive parameters: the formulation used modeling the freezing test performed, follows essentially Nishimura et al. [20].

Mass conservation of pore water is expressed as:

$$\frac{\partial}{\partial t}(\rho_l S_l \varphi + \rho_i S_i \varphi) + \nabla \times (\rho_l \mathbf{q}_l) = f^w \tag{6}$$

where φ is the porosity; S_l and S_i are degrees of liquid and ice saturation respectively ($S_l + S_i = 1$, as neither a gas phase nor cavitation is considered); $\mathbf{q}_l$ is the liquid water flux vector; and f^w is the sink/source term of mass. The water flux is calculated from generalised Darcy's law as:

$$\mathbf{q}_l = -\frac{k_r}{\mu_l}[k](\nabla P_l - \rho_l \mathbf{g}) \tag{7}$$

where $\mathbf{g}$ is the gravity acceleration vector, $[k]$ is the intrinsic permeability matrix, μ_l is the viscosity of liquid water, and k_r is the liquid phase relative permeability. Viscosity (Pa s) can be considered a function of the temperature, as:

$$\mu_l = 2.1 \times 10^{-6} \exp\left(\frac{1808.5}{273.15 + T}\right) \tag{8}$$

Relative permeability can be calculated from the expression:

$$k_r = \sqrt{S_l}\left[1 - \left(1 - S_l^{1/\lambda}\right)^{\lambda}\right]^2 \tag{9}$$

which can be derived from the van Genuchten function (Eq. (4)). The parameter λ is a material constant that in principle coincides

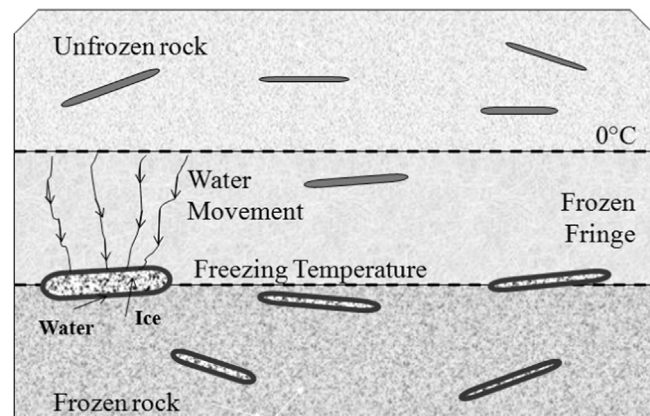**Fig. 1.** Idealization of freezing cracked rock: the sketch shows ice segregation at the boundary of the frozen fringe (T = 0°C) and the freezing front (T = Tf freezing temperature). Penny-shaped cracks are sub-parallel to the isotherms. Water migrates through the frozen fringe to growing ice-filled cracks (modified from Walder & Hallet, [16]).

with the parameter used in the retention curve and k_r varies between 0 and 1. The intrinsic permeability in the generalized Darcy's equation and the hydraulic conductivity $[K]$ (usually used in the flow equation when written in terms of piezometric head) are related by:

$$[K] = \frac{\rho_l g}{\mu_l}[k] \tag{10}$$

In the present study, all material properties have been considered isotropic.

The energy conservation equation is written as:

$$\frac{\partial}{\partial t}[e_s\rho_s(1-\varphi) + e_l\rho_l S_l\varphi + e_i\rho_i S_i\varphi] + \nabla \times (-\lambda_T\nabla T + \mathbf{j}_l^e) = f^e \tag{11}$$

where e_s, e_l and e_i are the specific internal energy of solid phase minerals, liquid water and ice respectively; λ_T is in this case the overall thermal conductivity of the material (consisting of soil minerals and pore materials); $\mathbf{j}_l^e$ is the advective term of heat flux ($\mathbf{j}_l^e = e_l\rho_l\mathbf{q}$); and f^e is the sink/production term of energy.

Fourier's law is employed in the above equation for calculating the conductive heat flux. The overall thermal conductivity λ_T is calculated by using the geometric mean:

$$\lambda_T = \lambda_s^{1-\varphi}\lambda_l^{S_l\varphi}\lambda_i^{(1-S_l)\varphi} \tag{12}$$

where the subscript s denotes the soil mineral phase. The specific internal energies, e_s, e_l and e_i, are:

$$e_s = c_s T \quad e_l = c_l T \quad e_i = -l + c_i T \tag{13}$$

where c_s, c_l and c_i are the specific heats for solid soil mineral, liquid water and ice respectively

Mechanical equilibrium can be written as

$$\nabla \times \boldsymbol{\sigma} + \mathbf{b} = 0 \tag{14}$$

where σ are total stresses and b are body forces.

4. Physical model

The experimental test developed was aimed at reproducing the ice lens growth mechanism due to the onset of ice segregation processes at the interface active layer-permafrost boundary. To achieve this goal, a long-term freezing test setup has been performed. The test reproduces the physical conditions in which ice action generates ice lenses just beneath the active layer of a homogeneous gneiss sample. The test was conducted on a cubic rock sample ($15 \times 15 \times 15$ cm) free of observable discontinuities and fissures, collected in Pelline Valley (Italy).

Given the small permeability of massive gneiss very long testing times were feared. Rotonda (1991) has shown that thermal microcraking increases rock porosity and therefore rock permeability without affecting significantly the rock strength. The adopted procedure to induce microcracking between adjacent crystalline grains or inside the grains was to subject the sample to three thermal heating cycles. In the first and third cycles the sample was slowly heated to a maximum temperature of 420 °C and cooled at a similar low rate (0.5 °C/min) in order to avoid thermal gradients inside the sample. In the second cycle the sample was slowly heated to 250 °C and cooled afterwards in a water bath. The unconfined compression strength of natural and thermally treated gneiss was measured in specimens drilled perpendicular to the gneiss foliation. The measured values were 113.3 MPa (natural gneiss, average of two tests) and 117.75 MPa (thermally treated sample, one test) suggest that the gneiss sample maintains the characteristics of a hard rock.

The porosity of the 150 mm cubic sample was not directly measured. Instead, it was indirectly determined by ultrasonic wave speed measurements following the relationships given by Willie et al. (1958) between wave velocities and physical properties of rock. In this approach the total wave transit time is the sum of the transit time in the mineral plus the transit time in the pore fluid. The total porosity has been calculated by inserting the P-waves velocities derived from ultrasonic measurements, a fluid velocity $v_f = 340$ m/s (Wyllie et al., 1958) and a rock matrix velocity $v_m = 6080$ m/s, which is an average velocity for the material characterized by a mixed mineralogy.

The calculated porosity ($\phi_0 = 0.15$), based on an indirect method, may lead to some error in calculations if compared with the original field porosity. Porosity enters into the two balance Eqs. (6) and (11), as a rate of change, which is controlled by the rock stiffness, and also by modifying the rates of change of degrees of saturation of water and ice. The first component will not change if the stiffness is maintained. The second component will modify the calculated times to reach a given state of the sample (steady state conditions, for instance) but it is not expected to modify the main results discussed in a next section.

Testing the ice segregation process requires specifically designed experiments. In order to simulate permafrost imposing a temperature gradient through the specimen equal to 1 °C/cm, the gneiss block has been placed on a basal cooling plate (Fig. 2). The sample was thermally insulated, as shown in the figure. The temperature distribution has been measured by a set of nine Pt100 platinum resistance thermometers. Eight sensors have been located on a vertical face of the specimen at different depths: 1.5, 3, 4.5, 6, 8, 10, 12, 14 cm (Fig. 2). An additional sensor was placed on the upper surface of the specimen. A thermal compound has been used to fill the air-gap between the thermosensors and the rough rock sample surface, in order to increase the thermal
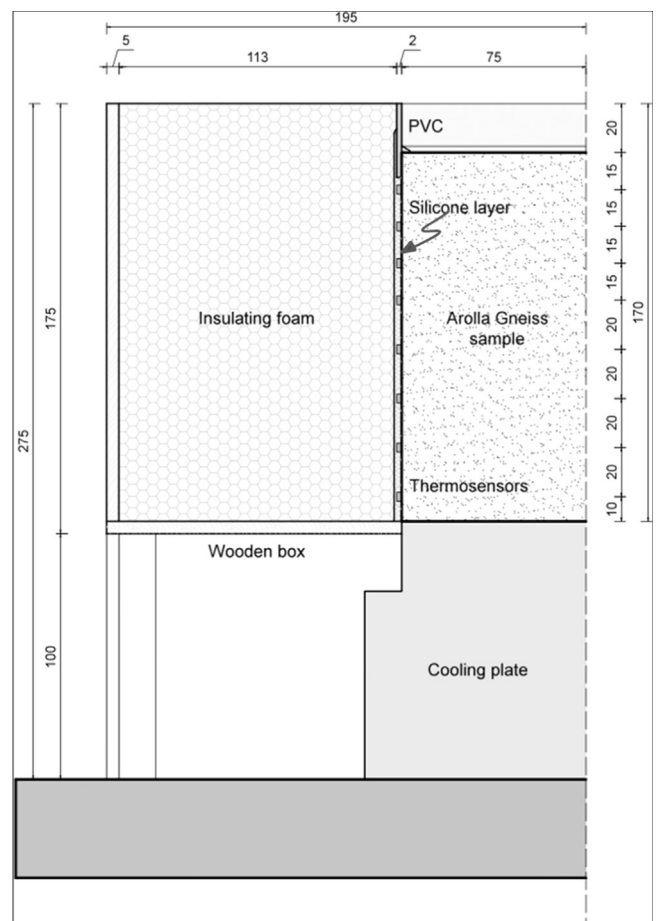

Fig. 2. Vertical cross section of experiment (dimensions are in millimeters).

conductivity at the interface. All the resistors were connected by means of shielded three-wire conductors to the acquisition system, which allows measurement, monitoring and storage of digital and analogue signals issued from electrical and physical sensors.

The lateral surfaces have been coated with a silicone layer to maintain the sample saturated during the test. Liquid water is drawn from the saturated upper surface into the rock sample. Lateral faces were covered by insulating material, 10 cm thick, to minimize lateral heat transfer and to ensure a one directional thermal gradient. Polyurethane foam was also sprayed inside a wooden box surrounding the sample and equipped with a suitable hole in the center, to allow placing the sample directly on the cooling plate (Fig. 2).

Since the presence of a nearby moisture source plays a fundamental role in ice segregation [6], a controlled supply of water has been guaranteed. A squared water pool has been fixed to the free upper surface of the sample and constantly kept full of water, so that a continuous downward water percolation could be available, ensuring a long-term (three months), slow freezing test under an open-system condition. An infrared lamp has been installed at a distance of 55 cm from the top of the sample to maintain a constant temperature of $+3\,°C$ on the upper surface.

5. Experimental results

At the end of a three month testing, ultra-sonic (US) measurements have been carried out on the sample, placing a P-wave transmitter-receiver on the upper surface of the cubic block: pulse transit time was recorded along the z-axis (normal to the isotherms). Fig. 3a shows the waveforms recorded when the sample was experiencing a linear temperature gradient, simulating the active-layer and the permafrost boundary. It is possible to note a reflection in the profile, at about 20 μs. Since the upper part of the sample was thawed, the depth of the reflecting element has been derived using a wave-velocity value equal to 4300 m/s (obtained from ultrasonic measurements). The calculated depth was about 4.3 cm.

It was feared that the measured reflection could be also induced by an internal ice-water front and not the result of the formation of a continuous ice layer. Therefore, it was decided to repeat later the same procedure by freezing the sample to $-15\,°C$, once the test was concluded. If the sample is frozen after the test the ice segregated layer and the cracks will remain in its original position.
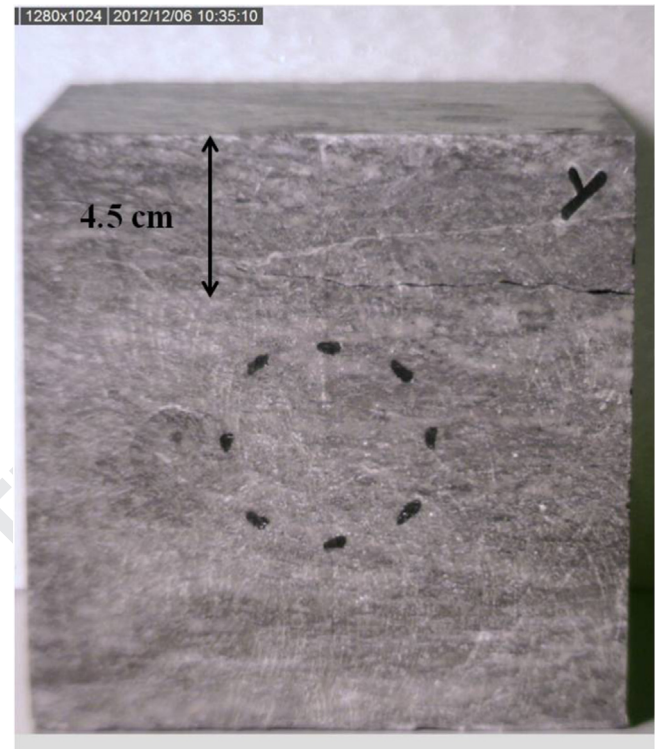

Fig. 4. Sub-horizontal crack at a depth of 4.5 cm observed on the sample sides after 3 months of testing.
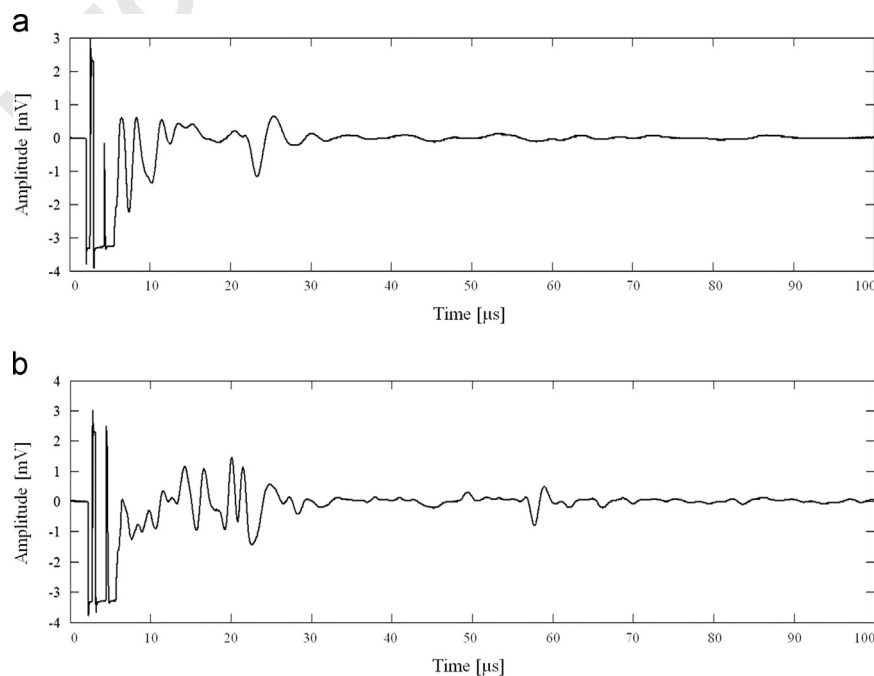

Fig. 3. P-wave signals recorded. (a) After a 3 month cooling period; (b) Once the sample was entirely frozen to -15ºC.

A reflection at about 27 µs has been measured (Fig. 3b) on the frozen sample: the corresponding depth was about 4.1 cm, using a wave-velocity value equal to 5500 m/s, obtained from ultrasonic measurements. It was concluded that the interface across which there was such a change in the elastic properties, which results in a reflection of the waveform profiles, was caused by a different reason: the presence of a millimeter-scale fracture as a consequence to ice segregation phenomena induced during the test.

The sample was then cleaned and freed from the insulating polyurethane layer and from the silicone sealing, with the purpose of examining its lateral surfaces. The picture in Fig. 4 shows a distinct crack at a depth of 4.5 cm. It was partially filled with continuous veins of ice.

Examined in more detail the block was found to have three distinct layers (see Fig. 4). The upper and the lower thirds of the gneiss cube lacked visible cracks; the lower part contained only pore ice, while the upper part was water saturated. On the contrary, the middle third was fractured and rich in segregated ice, at an average depth of 4.5 cm beneath the block surface. Distance of fractures to the upper face varied between 2.8 cm and 5.1 cm.

Microcracks had propagated horizontally through the gneiss, resulting in a continuous and thick macro-crack near the base of the upper active layer of the simulated permafrost, as shown in Fig. 5a and b. In some cases, filling of ice was visible inside the crack, despite the melting of the ice close to the rock surface induced by the sample cleaning. The ice was generally pure and white (bubble rich), as shown in Fig. 5c and d. Such bubbles are common in natural segregated ice [31], and they are perpendicular to the direction of heat and water flow during ice segregation.

The fracture was rough and sub-parallel to the cooling surfaces. The measured profile of steady state temperatures (reached after about three days of testing and kept during the experimental campaign), was essentially linear between the two upper and lower boundary conditions. The average position of the crack zone corresponds to the $-2\,^\circ$C isotherm. The ice-lens growth was observed at positions corresponding to a temperature range of $-0.5\,^\circ$C to $-2.5\,^\circ$C. This temperature range is consistent with Walder and Hallet theory [16]. Although they proposed an ice segregation temperature below $-5\,^\circ$C for hard rocks, characterized by low porosity (e.g. granite), this value entirely depends on the tensile strength of the rock, with weaker rocks (tensile strength around 2 MPa), breaking closer to 0 $^\circ$C. Considering the peculiarity of the thermally micro-cracked material that has been tested, the rock temperature range for the ice lens growth agrees essentially with literature data.

6. Finite element analysis of the physical model

The spatial domain of the plane strain problem was discretized by designing a two-dimensional structured FE mesh (15×15 cm), made of 225 quadrilateral elements and 256 nodes. This is a rather coarse mesh, but it was a compromise given the computational cost of a coupled Thermo Hydro Mechanical analysis. A uniform
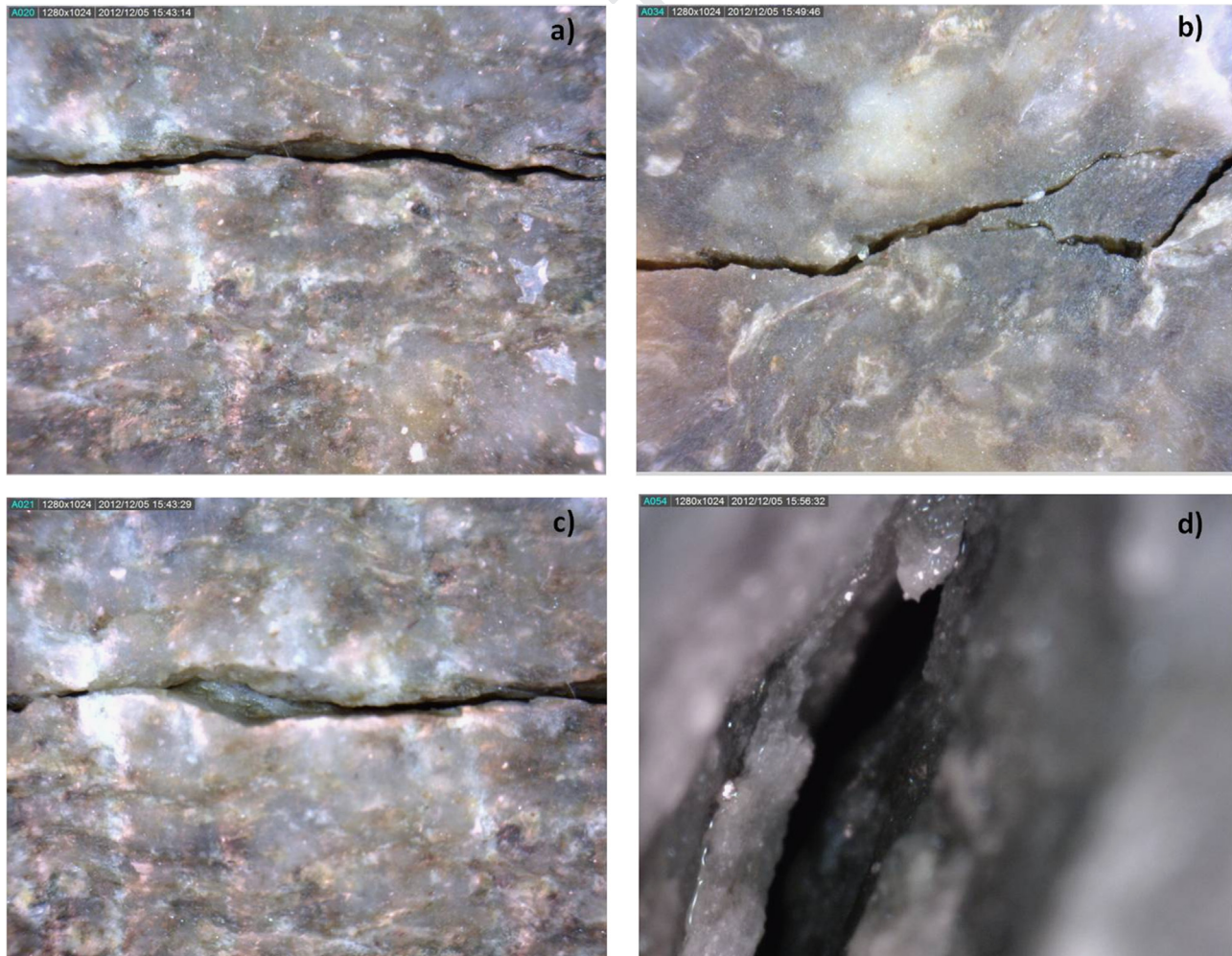

Fig. 5. (a), (b) Two aspects of the cracked zone around the freezing front; c), d) Details of the ice veins filling the open cracks.

temperature of 22 °C was assumed as the initial conditions in the analysis. The hydraulic boundary conditions along the top boundary were set to $P_l=0$, with the purpose of obtaining a hydrostatic pore water pressure distribution through the sample.

The bottom boundary temperature was reduced from 22 °C to -12 °C over the first seven hours, simulating the upward freezing, and was then kept constant, while the upper surface temperature was fixed at 3 °C. Zero heat flux/liquid flux conditions were specified along the lateral mesh boundaries.

Regarding the mechanical boundary conditions, a point was fixed at the lower boundary of the sample and the normal displacements were made equal to zero on the lower boundary. The remaining boundaries are stress free. Boundary conditions are sketched in Fig. 6.

6.1. Material parameters

The material parameters selected for input are summarized in Table 1. Gneiss thermal conductivity value has been obtained in laboratory tests carried out at the Institute of Geosciences and Earth Resources of Pisa on an Arolla gneiss rock sample. The specific heat value was set equal to 800 J/kg K [32]. Water and ice thermal conductivity and specific heat values have been derived from literature data: $\lambda_l=0.613$ W/m K [33], $c_l=4180$ J/kg K [33], and $\lambda_i=2.4$ W/m K [34], $c_i=2110$ J/kg K [34]. The specific latent heat of fusion was equal to 335,000 J/kg K [34].

There was a lack in knowledge of rock hydraulic properties: the parameters for the soil–water characteristic curve, P_0 and λ, were obtained by fitting Eq. (5) to the measured data determined by Borgesson and Hernelind for crystalline rocks [35]. A unique parameter λ was adopted for the water retention curve (Eq. (5)) and the relative permeability function (Eq. (4)).

Mechanical parameters were derived from laboratory tests carried out to determine strength and deformability under uniaxial conditions (MASTRLAB—Laboratorio Sperimentale Materiali e Strutture, Politecnico di Torino). The axial Young's modulus, E, has been calculated as the secant modulus at a stress level equal to 50% of the maximum strength ($E=78,000$ MPa). The Poisson's ratio has been determined as the ratio between the slope of the axial and the radial strain curves, at the same stress level ($\nu=0.2$). The unconfined compression strength of two samples oriented perpendicular to the foliation planes were 111.10 and 115.48 MPa, respectively.

Regarding plastic parameters, the value for the critical state parameter M was set to 2.25, which is equivalent to an angle of shearing resistance of 55°. This is a reasonable value for a gneiss
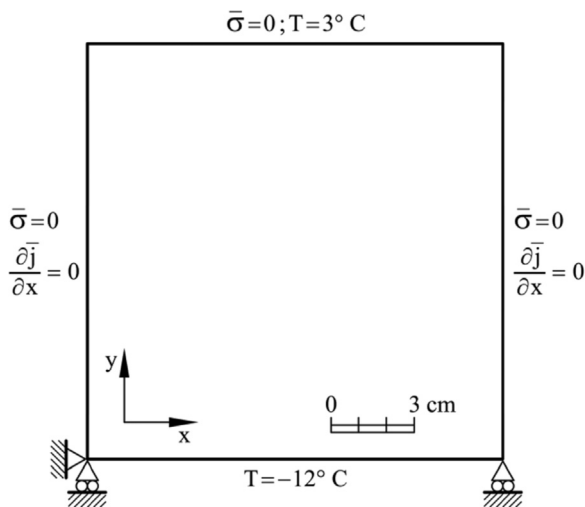

Fig. 6. Model sketch: discretized domain and boundary conditions.

Table 1
Material parameters.

| Property	Units	Value
Thermal		
Gneiss thermal conductivity, λ_s	W/m K	2.711
Water thermal conductivity, λ_l	W/m K	0.613
Ice thermal conductivity, λ_i	W/m K	2.4
Gneiss specific heat, c_s	J/kg K	800
Water specific heat, c_l	J/kg K	4180
Ice specific heat, c_i	J/kg K	2110
Specific latent heat of fusion, l	J/kg K	335,000
Hydraulic		
P_0	MPa	0.05
λ		0.5
Intrinsic permeability, k	m^2	1E−14
Relative permeability		0.5
Gneiss mechanical		
Young's modulus, E	MPa	78,000
Poisson's ratio, ν		0.2
Stress power, m		3.0
$\wp_0$	s^{-1}	100,000
c'	MPa	10
Critical state parameter, M		2.25
Other		
Gneiss mass density, ρ_s	kg/m^3	2759
Water mass density, ρ_l	kg/m^3	1000
Ice mass density	kg/m^3	916.4
Initial porosity	Φ_0	0.15
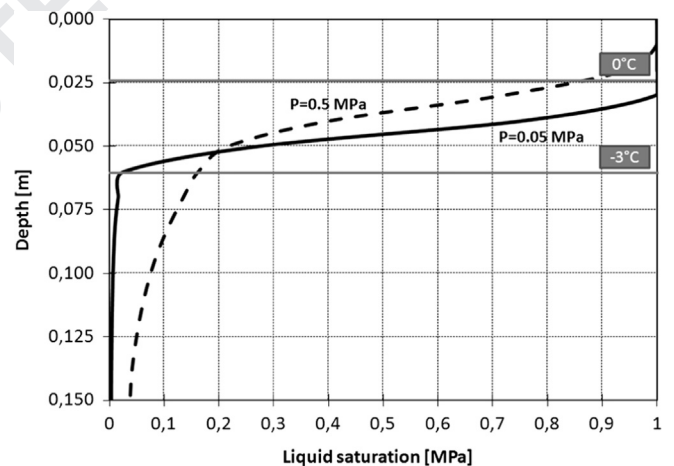
Fig. 7. Profiles of degree of liquid saturation calculated at steady state conditions, for two air entry values (solid line: P = 0.05MPa, dashed line: P = 0.5 MPa).

rock at low confining stress. It is also compatible with uniaxial compression and indirect tensile tests performed in the laboratory. The value of cohesion was set equal to 10 MPa. Finally, parameters m (stress power) and Γ_0 (viscosity) were set equal to 3 and 100,000 s^{-1}, respectively.

The solid phase density value corresponds to the density calculated from laboratory tests on thermally-cracked Arolla gneiss specimens (Department of Environment, Land and Infrastructure Engineering, Politecnico di Torino).

6.2. Model predictions

Two-dimensional freezing simulation was performed, in order to study the interactions between thermal, hydraulic and mechanical processes taking place in the sample. The temperature profile through the sample has been plotted in Fig. 7, once it reached thermal equilibrium after 24 h (solid line): very good fitting of the linear temperature prediction with laboratory data (dashed
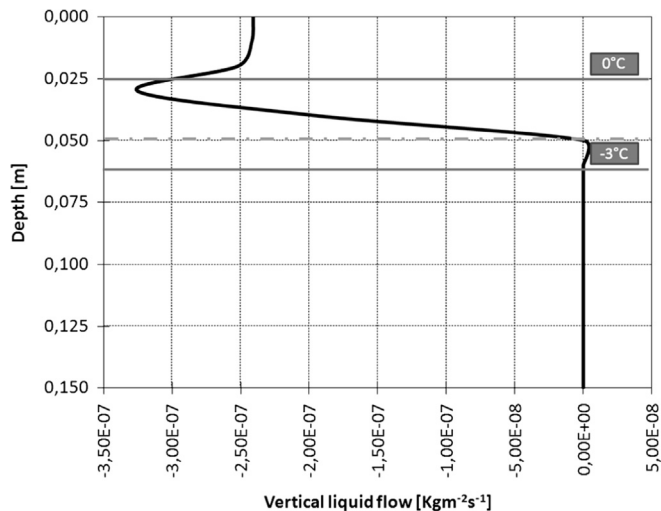
Fig. 8. Calculated liquid flux of water along the vertical direction 24 hours after the beginning of the freezing test.
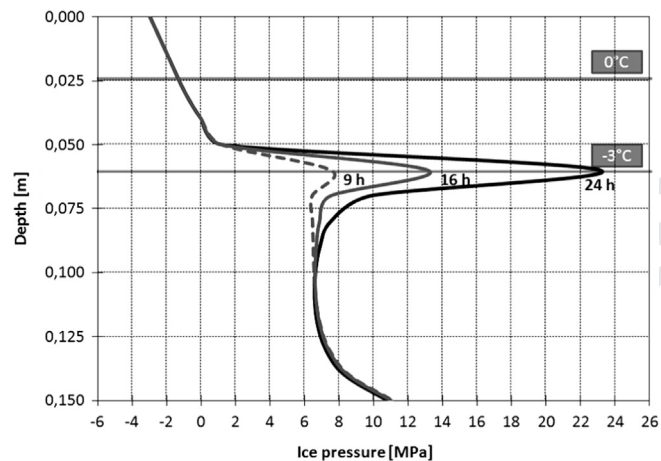

Fig. 9. Calculated profile of ice pressure for three different times after the beginning of the test: dashed grey line, 9 hours, solid grey line, 14 hours, solid black line, 24 hours (steady state) from the beginning of freezing.

line) can be observed. The zero-isotherm is located at a depth of 2.5 cm from the surface (Fig. 8).

Fig. 9 shows the variation of the liquid water degree of saturation with depth for an air entry value $P_0 = 0.05$ MPa (solid line). For temperatures in excess of 0 °C the pore water is in liquid phase ($S_l = 1$). Below 0 °C, S_l decreases fast. The phase change begins to occur at a depth of 3 cm for $T = -0.35$ °C. This temperature corresponds approximately to the "freezing point depression" in a variety of crystalline rocks [16].

It is possible to recognize a range between -3 °C and 0 °C in which a significant amount of water remains unfrozen. In this zone, the pore space in only partially ice-filled (S_l decreases from 1 to values close to 0). Borrowing the nomenclature of Miller [25], this zone is defined as a "frozen fringe". It occupies a band, 3.5 cm thick, limited by depths $z = 2.5$ cm and $z = 6$ cm. The temperature at the cold side of the frozen fringe is the effective freezing temperature (below -3 °C), and S_l is approximately equal to 0, i.e. the pore space is completely ice-filled. Above the frozen fringe, the rock is unfrozen ($S_l = 1$).

Fig. 9 also shows the effect of changing the air entry value (parameter P in Eqs. (4) and (5). If P is increased from the adopted values in calculations ($P = 0.05$ MPa) to $P = 0.5$ MPa, the rock does

not desaturate i.e. the space in the pores is not completely filled with ice. Varying proportions of liquid water remains in all points (dashed line in Fig. 9).

The computed liquid flux along the y-axis obtained after 24 h from the beginning of freezing is shown in Fig. 10. The figure provides an instantaneous picture of the flow distribution in the sample during the initial transient phase. Flow rates are controlled by the boundary inflow, the changes of Sl along the sample and the sink provided by the crystallization of ice. The plot shows how the accumulation of freezing pore water drives the ice segregation process: the unfrozen pore water is drawn from the surface into the frozen fringe. The flux increases gradually from the freezing front down to the frozen fringe, and it reaches a maximum value of $3.25E - 07$ kg/m²/s² at a depth of 3 cm. At a depth of 5 cm, the flux essentially vanishes as the unfrozen water film between ice and solid rock tends to migrate toward the frozen rock.

It can be noticed that a temperature of -3 °C is the critical value which controls permeability and therefore, water migration: slightly below this value, i.e. for depths in excess of 6 cm, the flow almost vanishes, marking the boundary between frozen fringe and
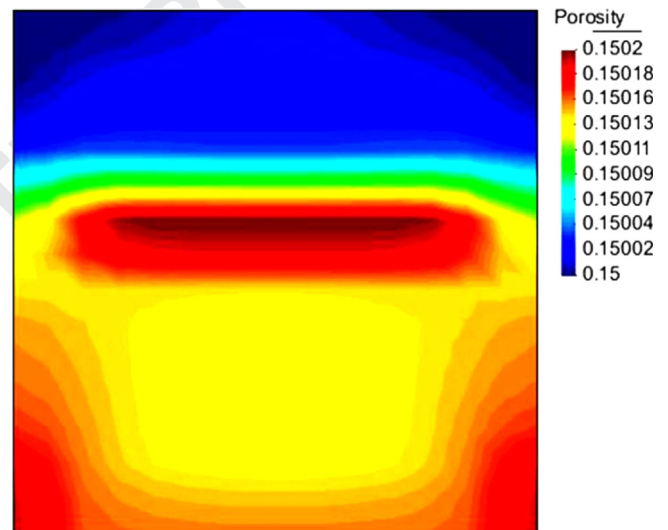

Fig. 10. Map of sample porosity, 24 hours from the beginning of freezing (steady state).
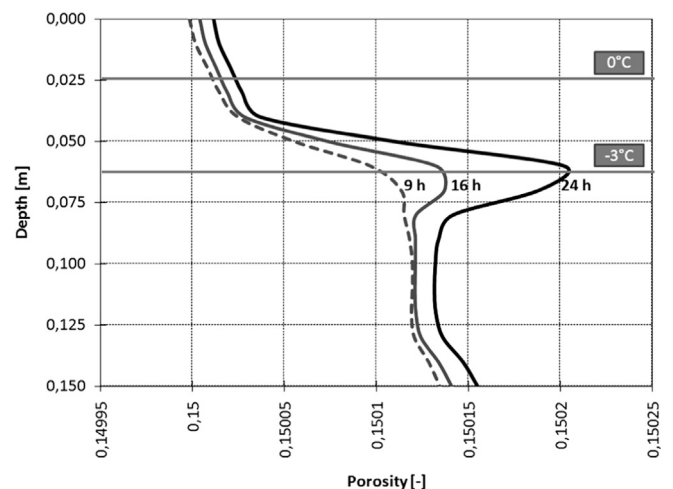

Fig. 11. Vertical profiles of calculated porosity at three different times after the beginning of the test: dashed grey line, 9 hours, solid grey line, 14 hours, solid black line, 24 hours (steady state) from the beginning of freezing.
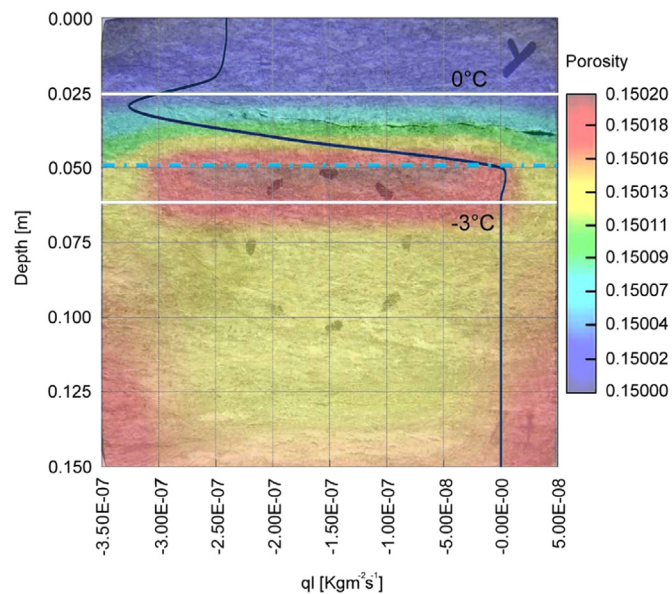
Fig. 12. The figure was made superimposing a sample photograph showing the position of the dominant crack, the calculated porosity and the vertical flow rate. Also indicated is the position of the 0ºC and -3ºC isotherms.

completely frozen rock. At this depth, which corresponds to the isotherm $-3\,°C$, a maximum value of ice pressure is calculated ($P_i = 23$ MPa), as shown in Fig. 11 (solid line: steady state after 24 h from the beginning of freezing).

If temperatures remain above $-3\,°C$, the frozen fringe is relatively permeable, and the fluid flow reaches the maximum value equal to $3.25E-07$ kg/m/^{2}s/^{2}. At lower temperatures ($T=-3\,°C$), the maximum ice pressure is quite large, but the liquid flux is definitely reduced due to the extremely low hydraulic conductivity of the frozen fringe there. Sustained freezing should be most effective when temperature is around $-3\,°C$: higher temperatures prevent ice pressure from building up sufficiently to produce significant crack growth, but at lower temperatures, the migration of water necessary for sustaining crack growth is strongly inhibited. The result is in general agreement with literature data, which suggested that the temperature at which ice segregation induces microgelivation in medium porosity hard rocks is lower than $-3\,°C$ [6]; Hallet et al. [37] also recognizes that most of the fracture activity (and consequently AE generation) occurs at temperature between $-3\,°C$ and $-6\,°C$.

A map of the simulated porosity change is presented in Fig. 12. A small increase of porosity from the initial value of 0.15 is visible at depth of 6 cm, demonstrating how the accumulation of freezing pore water reaches a maximum in this critical zone. As a matter of fact, the unfrozen pore water is drawn into the freezing front: in Fig. 12 the profile of porosity as a function of depth is shown for three different time steps (i.e. 9, 14 and 24 h from the beginning of freezing). It is interesting to note that the highest porosity value for each step coincides with the $-3°$ isotherm depth and that this peak value increases with time. In fact, after the transient cooling, freezing at fixed temperature gradient allows the localization of increasing porosity precisely in that area, which should therefore be the preferential place for the ice lenses formation [5]. Calculated maxima of ice pressure and porosity change (Figs. 11 and 12) are located on the same position.

The observed fracture depth (Fig. 12) is located within the "active" layer or "frozen fringe" zone at depths varying between 2.5 and 6 cm. The position of this fracture is not exactly located at the calculated position of the maximum change in porosity but the model provides a reasonably good prediction.

7. Discussion and conclusions

Permafrost conditions in Central Europe high mountain areas have experienced changes in recent years which have been associated with climatic change although other factors may be involved. Observations indicate that freezing conditions are permanently maintained at some depth within the rock but the impact of warm and wet weather leads to a supply of liquid water on the exposed rock surfaces. As a result, liquid water is attracted towards the permafrost boundary where it changes phase and crystallizes as ice.

However, one of the open questions was to know if ice crystallization required pre-existing discontinuities or, else, it could crystallize in pores and, in addition, it was able to induce rock damage, generating local cracks which eventually would coalesce into larger fissures. These fissures will be progressively filled with continuous ice. In this way weak discontinuities will be formed in a direction parallel to the permafrost boundary increasing the risk of rock falls.

High mountain rocks are hard and exhibit a low porosity/microcracking. The intact sample tested, a dense low porosity gneiss, is representative of rockmass conditions at high altitudes (more than 3000 m a.s.l.). The long term test performed has confirmed the development of a continuous open crack within a permafrost fringe bounded by the isotherms $0\,°C$ and $-3\,°C$. Within this range ice and liquid water coexist. This is a zone where cryogenic suction attracts water from the warm boundary. Some field observations reported in the paper are consistent with laboratory observations.

An additional interesting finding is that the formulation for ice-water interaction in porous soils, directly based on the coupled flow deformation analysis of unsaturated soils is capable of reproducing the main features of the phenomenon. The formulation has been outlined in the paper and model parameters have been approximated from known physical constants and experiments on the gneiss rock tested. The most relevant result is that the model predicts the location and size of the frost fringe and, also, the approximate position of the ice-filled crack. Note, however, that the model does not have provisions for modeling rock fracture and it describes, during the entire test, a porous material. Nevertheless, it is believed that that the model used provides a reasonable approximation to ice-liquid interactions in hard micro-fractured porous rocks.

Uncited reference

[36].

References

[1] Krautblatter M, Funk D, Gunzel FK. Why permafrost rocks become unstable: a rock-ice mechanical model in time and space. Earth Surf Process Landforms, under rev.
[2] Haeberli W, Wegmann M, von der Muhll D. Slope stability problems related to glacier shrinkage and permafrost degradation in the Alps. Eclogae Geol Helv 1997;1997(90):407–14.
[3] Fischer L, Huggel C. Methodical design for stability assessments of permafrost-affected high-mountain rock walls. In: Proceedings of the ninth international conference on Permafrost. Fairbanks; 28 June–3 July 2008. p. 439–44.
[4] Fischer L, Amann F, Moore JR, Huggle C. Assessment of periglacial slope stability for the 1988 Tschierva rock avalanche (Piz Morteratsch, Switzerland). Eng Geol 2010;116:32–43.

[5] Matsuoka N, Murton J. Frost weathering: recent advances and future directions. Permafrost Periglac 2008;19:195–210.

[6] Matsuoka N. Microgelivation versus macrogelivation: towards bridging the gap between laboratory and field frost weathering. Permafrost Periglac 2001;12:299–313.

[7] Noetzli J, Hoelzle M, Haeberli W. Mountain permafrost and recent Alpine rockfall events: a GIS-based approach to determine critical factors. In: Proceedings of the eighth international conference on permafrost. Zurich; 21–25 July 2003. p. 827–32.

[8] Deline P. Recent Brenva rock avalanches (Valley of Aosta): new chapter in an old story? Suppl Geogr Fis Dinam Quat 2001;15:55–63.

[9] Ravanel L, Allignol F, Deline P, Gruber S, Ravello M. Rockfalls in the Mont Blanc massif in 2007 and 2008. Landslides 2010;7:493–501.

[10] Deline P, Jaillet S, Rabatel A, Ravanel L. Ground-based LiDAR data on permafrost-related rock fall activity in the Mont Blanc massif. In: Proceedings of the ninth international conference on permafrost. Fairbanks; 28 June–3 July 2008. p. 349–54.

[11] Ravanel L, Deline P. Climate influence on rockfalls in high Alpine steep rockwalls: the North side of the Aiguilles de Chamonix (Mont Blanc massif) since the end of the 'Little Ice Age'. Holocene 2012;21(2):357–65.

[12] Beniston M. Climate change in mountain regions: a review of possible impacts. Clim Change 2003;59:5–31.

[13] Amitrano D, Arattano M, Chiarle M, Mortara G, Occhiena C, Pirulli M, Scavia C. Microseismic activity analysis for the study of the rupture mechanisms in unstable rock masses. Nat Hazard Earth Syst Sci 2010;10(4):831–41.

[14] Duca S. Design of an experimental procedure and set up for the detection of ice segregation phenomena in rock by acoustic emissions. Italy: Politecnico di Torino; 2013 PhD thesis.

[15] Murton JB, Peterson R, Ozouf JC. Bedrock fracture by ice segregation in cold regions. Science 2006;314:1127–9.

[16] Walder JS, Hallet B. A theoretical model of the fracture of rock due to freezing. Geol Soc Am Bull 1985;96:336–46.

[17] Whalley WB, Bruce BR, Rainey MM. Weathering, blockfields and fracture systems and the implications of long-term landscape formation: some evidence from Lingen and Oksfordjokelen areas in North Norway. Polar Geogr 2004;28:93–119.

[18] Matsuoka N. Mechanism of rock breakdown by frost action: an experimental approach. Cold Reg Sci Technol 1990;17:253–70.

[19] Ondrasina L, Kirchner D, Siegesmund S. Freeze-thaw cycles and their influence on marble deterioration: a long-term experiment. Geol Soc London Spec Publ 2002;205:9–18.

[20] Nishimura S, Gens A, Olivella S, Jardine RJ. THM-coupled finite element analysis of frozen soil: formulation and application. Géotechnique 2009;59(3):159–71.

[21] Olivella S, Carrera J, Gens A, Alonso EE. Nonisothermal multiphase flow of brine and gas through saline media. Transp Porous Media 1994;15(3) 271-29.

[22] Olivella S, Gens A, Carrera J, Alonso EE. Numerical formulation for a simulator CODE_BRIGHT for the coupled analysis in saline media. Eng Comput 1996;13(7):87–112.

[23] Gens A, Garcia Molina AJ, Olivella S, Alonso EE, Huertas F. Analysis of a full scale in situ test simulating repository conditions. Int J Numer Anal Met 1998;22(7):515–48.

[24] Koopmans RWR, Miller RD. Soil freezing and soil water characteristic curves. Soil Sci Soc Am J 1996;30(6):680–5.

[25] Miller RD. Frost heaving in non-colloidal soils. In: Proceedings of the third international conference on permafrost. Edmonton; 10–13 July 1978. p. 708–13.

[26] Black PB, Tice AR. Comparison of soil freezing curve and soil water curve data for Windsor Sandy Loam. Water Resour Res 1989;25(10):2205–10.

[27] Grant SA, Sletten RS. Calculating capillary pressure in frozen and ice-free soils below the melting temperature. Environ Geol 2002;42(2-3):130–6.

[28] Coussy O. Poromechanics of freezing materials. J Mech Phys Solids 2005;53(8):1689–718.

[29] Fredlund DG, Xing A. Equations for the soil–water characteristic curve. Can Geotech J 1994;31(4):521–32.

[30] van Genuchten MT. A closed form equation for predicting the hydraulic conductivity of unsaturated soils. Soil Sci Soc Am J 1980;44:892–8.

[31] Murton JB, Coutard JP, Ozouf JC, Lautridou JP, Robinson DA, Williams RBG. Experimental design for a pilot study on bedrock weathering near the permafrost table. Earth Surf Proc Land 2000;25:1281–94.

[32] Williams PJ, Smith MW. The Frozen Earth, fundamentals of geocryology. Cambridge: Cambridge University Press; 1989.

[33] Cengel YA. Heat transfer: a practical approach. New York: McGraw-Hill; 2003.

[34] Schulson M, Duval P. Creep and fracture of ice. Cambridge: Cambridge University Press; 2009.

[35] Borgesson L, Hernelind J. Coupled thermo-hydro-mechanical calculations of the water saturation phase of a KBS-3 deposition hole. Influence of hydraulic rock properties on the water saturation phase. SKB report TR-99-41, Stockholm; 1999.

[36] Wyllie MRJ, Gregory AR, Gardner GHF. An experimental investigation of factors affecting elastic wave velocities in porous media. Geophysics 1958;23:459–93.

[37] Hallet B, Walder JS, Stubbs CW. Weathering by segregation ice growth in microcracks at sustained sub-zero temperatures: verification from an experimental study using acoustic emissions. Permafrost Periglac 1991;2:283–300.